Residual strength assessment and destructive testing of decommissioned concrete bridge beams with corroded pretensioned reinforcement

Rhys A. Rogers, Liam Wotherspoon, Allan Scott, and Jason M. Ingham

- Destructive tests were performed on 19 decommissioned pretensioned concrete bridge beams that had corroded pretensioned reinforcement. The beams were from the 1969 Tiwai Point Bridge in Southland, New Zealand.
- The condition of the beams tested ranged from good condition to those with severe corrosion in 4 of the 21 prestressed strands.
- A proposed methodology for assessment of the residual strength of beams with corroded pretensioned reinforcement was shown to provide an effective means of estimating the number of corroded strands that should be disregarded in calculation of the residual strength.

Recent deterioration of prestressed concrete bridge beams in New Zealand and around the world highlights an escalating problem.[1–3] Corrosion of pretensioned reinforcement is especially critical because of the highly stressed nature of these structures; a small amount of corrosion of a pretensioned strand results in a considerable reduction in the structural capacity of the member.

The Tiwai Point Bridge is located in a highly aggressive coastal environment in the South Island of New Zealand. The structure was opened to traffic in 1969 and replaced in 2009–2010 because of severe corrosion of the pretensioned reinforcement. Nineteen of the 42-year-old beams were set aside as test specimens for a destructive and nondestructive testing program.

This paper forms part of a larger study that aims to develop a methodology for nondestructive assessment of the residual strength of beams that have experienced corrosion of pretensioned reinforcement. Opportunities to measure the capacity of full-scale beams with corroded pretensioned reinforcement are relatively rare, and although a number of testing programs have been conducted around the world, each study provides only a small number of actual destruc-

tive test data points.[2,3] The deconstruction of the Tiwai Point Bridge allowed for a large number of destructive tests to be performed on identical beams with varying degrees of corrosion damage. The large number of related destructive test data points will be used to develop and assess the accuracy of nondestructive residual strength evaluation methodologies in later parts of the larger study.

A summary of nondestructive corrosion assessment procedures used is presented, along with results from the destructive testing program. The measured flexural capacity of each beam is correlated to observed corrosion damage and compared with the measured flexural capacity of good-condition beams of the same design. A nondestructive methodology for estimation of the residual strength of the corroded beams is proposed, but no attempt to verify this model is presented here. Future work will aim to develop this methodology so that it can be used to reliably assess the residual strength of corroding pretensioned bridge beams of other designs. The accuracy of the methodology will be verified both numerically and by applying it to the destructive test results from this study and to those found in the literature.

Tiwai Point Bridge

Background

The Tiwai Point Bridge is located at latitude S46° 34′ near the southern tip of the South Island of New Zealand. The bridge was constructed specifically to serve an aluminum smelter and provides the only road access to the facility. The smelter is one of the largest single industrial operations in the country and accounts for a large proportion of the local region's economy.[4]

The electronic weather station located on Tiwai Point approximately 4 km (2.5 mi) from the bridge site recorded daily climate data for the entire service life of the structure. The absolute minimum and maximum temperatures recorded between 1969 and 2010 were -5.2°C and 32.1°C (23°F and 90°F) respectively. The monthly average of daily minimum temperatures recorded over the life of the structure was lowest in July, at 2.9°C (37°F), and highest in January and February at 10.9°C (52°F). An average of 12 days per year were recorded as screen frost days, defined as a day on which the air temperature dropped below 0°C (32°F) inside a standard Stevenson screen enclosure located 1.3 m (4.3 ft) above the ground.

The bridge site is 3.5 km (2.2 mi) away from the nearest open surf beach; however, the structure itself is 500 m long (1640 ft) and with adjoining causeways crosses a 1 km wide (0.6 mi) section of Awarua Bay, which is affected by strong prevailing southwesterly winds. The soffit of the superstructure was 3.7 m (12 ft) above mean sea level,[5] and the mean tidal range in the bay varies from 1.5 to 2.21 m (4.9 to 7.25 ft).[6] Average monthly wind speeds recorded during the life of the structure varied from 4.5 m/sec (15 ft/sec) in July to 6.9 m/sec (23 ft/sec) in November, and the annual average number of days with wind gusts in excess of 12.3 m/sec (40.4 ft/sec) was 222. The Beaufort scale describes sea conditions for given wind speeds, and although it does not directly apply to harbors or estuaries, it does give an indication of the conditions that can be expected on a wide body of water affected by the wind. The scale reports that in winds of 3.4 to 5.4 m/sec (11 to 18 ft/sec), scattered whitecaps can be expected. In winds of 10.8 to 13.8 m/sec (35.4 to 45.3 ft/sec), white foam crests are extensive, large waves begin to form, and some spray can probably be expected.[7] These conditions provided an aggressive environment due to the regular presence of wind-blown salt spray, which resulted in chloride buildup on the structure.

Although the bridge is on a public road, it leads only to the aluminum smelter and a small picnic area, so the regular traffic volume is low and easily defined. A count in 2005 recorded 30 heavy vehicles per day,[8] the majority of which were semiarticulated trucks carrying the maximum allowable load of smelted aluminum to the domestic market. Raw material for smelting and product bound for the international market were transported by sea directly from the wharf adjoining the smelter. Other regular traffic included three buses in and out of the plant twice a day carrying staff members and a small number of light vehicles carrying staff and contractors. Occasionally the bridge was subjected to overloads because no alternative land route was available, particularly during construction and maintenance operations at the smelter.

Design and construction

The bridge was originally designed for the more severe of two loading cases: the H20-S16-T16 design loading standard or a single 100-ton (91-tonne) truck load restricted to travel over the central five beams.[9] The H20-S16-T16 loading cases encompassed traffic loads experienced during normal service of the bridge, while the 100-ton overload case allowed for the delivery of supplies and equipment required for construction and maintenance of the aluminum smelter.

The bridge consisted of twenty-seven 18 m long (59 ft) spans, each of which contained nine 686 mm (27.0 in.) deep precast concrete T beams transversely posttensioned together. The beams contained both pretensioned and posttensioned longitudinal reinforcement and mild steel transverse reinforcement. No additional corrosion protection was provided to the stressed or mild reinforcement other than that from the 57 mm (2.2 in.) specified concrete cover. The specified 28-day compressive strength of the concrete was approximately 38 MPa (5500 psi), but no other information on the concrete is available.[9]

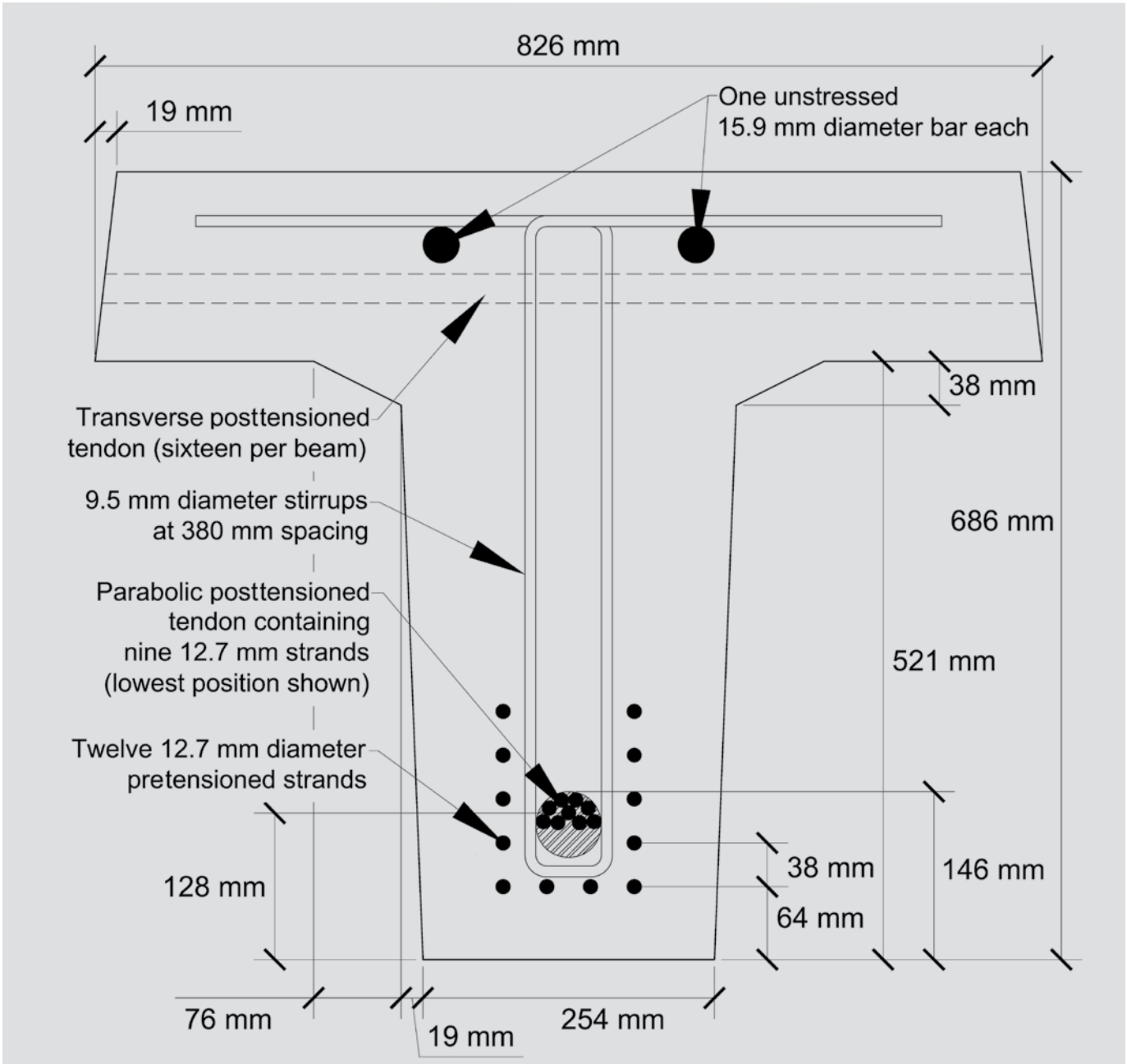

Figure 1. Typical beam cross section with posttensioned tendon duct shown at lowest point of parabolic drape. Note: 1 mm = 0.0394 in.

Each of the five central beams contained twelve 12.7 mm diameter (0.500 in.) pretensioned strands, while each of the two outside beams on both sides contained 10 pretensioned strands. All beams contained one draped posttensioned tendon with nine 12.7 mm diameter strands. Each posttensioned tendon extended four spans between anchors and served to provide some continuity between spans, and expansion joints were located between spans with anchors. The beams with an expansion joint at one end had a shallower parabolic drape to accommodate the anchor and a different moment envelope. The difference between the highest and lowest points of the parabolic drape was 454 mm (17.9 in.) for beams with an expansion joint at one end and 489 mm (19.3 in.) for those without.

The different pretension and posttension arrangements resulted in four beam types on the bridge, each with different longitudinal pretensioning configurations and thus considerably different ultimate limit state behaviors. In order from strongest to weakest, the four beam types can be identified as: 12 pretensioned strands without an expansion joint, 12 pretensioned strands with an expansion joint, 10 pretensioned strands without an expansion joint, and 10 pretensioned strands with an expansion joint.

Figure 1 shows a typical cross section of a beam. An important feature of the design was that the transverse reinforcement does not enclose the pretensioned strands. This detail allows the more critical pretensioned longitudinal

reinforcement to corrode before the mild steel transverse reinforcement.[1] This results in a greater loss of structural capacity at the time when corrosion causes cracking of the concrete and becomes visible on the surface.

The bridge was constructed as part of the development of the Tiwai Point Aluminium Smelter, which also included the construction of a dedicated wharf. The wharf structure consists of a pier head and a single-lane access bridge. The superstructure of the access bridge is of similar design to the Tiwai Point Bridge. Both structures were constructed using the steel launcher and gantry system (**Fig. 2**).

Service life and inspection history

During its service life, the Tiwai Point Bridge was subjected to routine inspections on a two- to four-year cycle. These inspections involved visual assessment of the bridge and fixtures from the roadway and abutments.As a result of these inspections, several maintenance operations were conducted on the railings and other fixtures as they were identified. The regular inspection procedure allowed only for cursory inspection of the underside of the deck and beams because no means of access was available.

Measurements of the depth-to-bed level at each pile set were taken in 2000 to check for changes in the bed profile or scour around the piles. During this work extensive deterioration of the structure was noted, and as a result a full inspection of the structure by boat was performed. The inspection revealed reinforcement corrosion, which was a result of chloride ingress and was evidenced by longitudinal cracking along the sides of the beams at the level of the bottom layer of pretensioned strands. After a thorough investigation, it was estimated that in the worst cases this cracking correlated to a loss of up to 60% of the cross section of the bottom layer of pretensioned strands.[4] Several visual inspections were conducted to determine the prevalence of this damage. The most recent inspection, in 2007, revealed longitudinal cracking in 55 of the 243 beams.[10]

Figure 2. Tiwai Point Bridge launcher in operation in 1967. Photo courtesy of Ray Price.

Figure 3 shows evidence of longitudinal cracking and rust staining in three beams from the same span and similar cracking in one beam. The maximum measured width for this type of crack was 5 mm (0.20 in.), and the cracking was consistently at the level of the bottom layer of pretensioned reinforcement.

Overloads were no longer permitted on the bridge after initial detection of the damage, and weight and speed limits of 80% Class 1 loading and 30 kph (20 mph) were applied to heavy traffic in 2004. After replacement was scheduled in 2006 the limits were relaxed to 100% Class 1 and 30 kph (20 mph) because consideration of the long-term effects of overstressing the bridge was no longer required.[8]

Corrosion-induced cracking in three beams from one span

Close-up of corrosion crack in one beam

Figure 3. Examples of corrosion-induced longitudinal cracking.

The original superstructure of the bridge was decommissioned and replaced in 2009 and 2010 because widespread and severe corrosion of the pretensioned strands was identified in the beams. The piers and pile caps were also in a deteriorated state, but these elements were rehabilitated and reused.

Nondestructive testing

The aim of the nondestructive testing program was to identify and quantify the corrosion in the pretensioned strands within each concrete beam. This information was used to estimate the amount of effective pretensioned reinforcement for comparison with the destructive test results. This section gives an overview of the nondestructive testing techniques employed. **Table 1** summarizes the results.

Visual inspection

A detailed visual inspection was performed, and any identified defects were mapped and photographed. Details specific to each beam were recorded, such as the width of flanges, pull-in of cut posttensioning tendons, and hog in beams.

Visual inspection resulted in identification of small patch repairs on some of the beams from remedial work to address corrosion of stirrups and metal debris cast into the concrete. These repairs were concentrated in the haunches and in the soffit of the webs. Small areas of poor compaction were evident in many of the beams, but these locations did not reliably coincide with areas of visible corrosion. A high proportion of beams had some minor cracking and spalling evident on the sides of the haunches, consistent with corrosion of stirrups, which had lower design cover in this region. In 8 of the 19 tested beams, longitudinal cracks along the sides of the web were evident at the elevation of the pretensioned reinforcement. This cracking was often accompanied by rust staining and was caused by corrosion of the pretensioned reinforcement.

Following destructive testing of the beams, a survey of the corrosion damage was taken in the area of broken concrete around the failure plane. The survey identified varying degrees of corrosion of the pretensioned strands, almost exclusively occurring in those strands located in the bottom layer of reinforcement. No damage to the strands or duct making up the posttensioned tendons was found, and the duct was well grouted in all inspected areas. In several cases, some light surface corrosion was noted on the posttensioned strands; however, in these cases it was confirmed that there was no loss of cross section on any of the strands or wires in the tendon.

Cover depth survey

A cover survey was performed using an electromagnetic cover meter to determine the depth of cover to the pretensioned reinforcement and stirrups. The results indicated that the average cover to the pretensioned strands was 59 mm (2.3 in.). The minimum measured cover to strands was 38 mm (1.5 in.), and the average of the minimum strand cover measured in a given beam was 50 mm (2 in.). External evidence of strand corrosion was not found in the areas with the lowest cover depth readings.

Cover to stirrups was measured only in the haunches because this was the only area where stirrups were nearer to the surface of the concrete than the pretensioned reinforcement. The average measured cover to stirrups was 39 mm (1.5 in.), the lowest measured cover depth was 14 mm (0.55 in.), and the average of the minimums was 24.5 mm (0.965 in.). Low cover depth correlated strongly to external evidence of stirrup corrosion.

Electro-potential mapping

Electro-potential mapping (EPM) measures the difference in potential between the reinforcement embedded in the concrete and a copper/copper sulfate reference electrode embedded in a handheld sensor. The measured potential is considerably more negative in areas of active corrosion of the reinforcement.[11] EPM was performed on the sides of the web and the soffit to identify sites of active corrosion that were not visible on the surface of the concrete. While no strand corrosion was identified in areas without cracking, EPM assisted in the location of fine longitudinal cracks that had gone unnoticed in the visual inspection. Neither the corrosion rate nor the extent of deterioration can be determined using this method.[12]

EPM results were analyzed and showed a strong correlation with visual signs of corrosion, such as longitudinal cracking in the sides of the web. Regions identified as corroding by EPM correlated closely with regions of strand failure.

Figure 4 gives an example of an electro potential map of the web of a beam. The beam has been cut into four sections so that the entire length can be shown in one figure. Each column represents five readings at one section of the beam, two readings from each side of the web, and one from the soffit. Red cells indicate areas with a high likelihood of corrosion, yellow and orange indicate some likelihood, and green cells indicate low likelihood.

In this case there is an area of active corrosion just south of the centerline, and some likelihood of corrosion at the south end of the beam. In the destructive test, beam 2C displayed flexural failure in the red EPM region, and breakout of the concrete after the test confirmed that all four of the bottom pretensioned strands were severely corroded and unable to carry load. While the electro potential maps had a strong correlation with sites of active corrosion, in this study they did not provide significantly more insight than a thorough nondestructive visual inspection would have.

Table 1. Summary of nondestructive testing results compared with postfailure breakout

Beam type	Beam label	Visual inspection			Electro potential mapping west		Electro potential mapping east		Postfailure breakout			
		Longitudinal cracking visible on side of web	Maximum crack width west,* mm	Maximum crack width east,* mm	Maximum in failure zone	Average over 0.5 m in failure zone	Maximum in failure zone	Average over 0.5 m in failure zone	Peak load, kN	Number of corroded strands†	Failure location from centerline, m	Dominant failure mode
12 pretensioned strands, no expansion joint	14G	Neither	0	0	282	254	272	246	346	0	4.5 north	Shear
	3C	Neither	0	0	187	177	205	184	338	0	4.5 north	Shear
	18E	Both	>2	>2	621	526	573	532	266	4	2 north	Flexural
	21F	Both	2	3	577	526	494	449	260	3	1.5 south	Flexural
	3D	Both	5	4	555	452	577	445	246	3.29	1.3 south	Flexural
	2C	Both	3	3	572	442	509	430	233	4	1.4 south	Flexural
12 pretensioned strands, expansion joint	13F	Neither	0	0	189	177	174	163	317	0	Reached maximum stroke	
	1D	Neither	0	0	171	124	190	178	310	0	2 north	Flexural
	4D	West	3	0	483	414	430	384	290	2.43	1.7 south	Flexural
	16G	Both, not at same section	>2	>2	401	348	344	330	288	2.14	1.5 south	Flexural
	16F	Both	>2	>2	476	418	460	389	215	4	1.5 south	Flexural
10 pretensioned strands no expansion joint	3B	Neither	0	0	182	172	210	197	311	0	1.5 south	Flexural
	2B	Neither	0	0	201	175	188	177	300	0	2 south	Flexural
	21I	West	5	0	461	415	340	280	270	1	1.4 south	Flexural

* Beams that underwent testing early in the program did not have accurate crack width measurements.

† The whole number represents completely corroded strands. The number after the decimal point represents partial damage to one strand, expressed as the number of corroded wires divided by 7. No beam had partial damage to more than one strand.

Note: 1 mm = 0.0394 in.; 1 m = 3.28 ft; 1 kN = 0.225 kip.

Chloride ingress

Chloride content tests measure the ingress of chlorides into concrete. Chlorides from salt water diffuse into the concrete, and when the concentration at the depth of reinforcement reaches the threshold value, corrosion can initiate. Chloride ingress was the principal cause of reinforcement corrosion on the Tiwai Point Bridge.

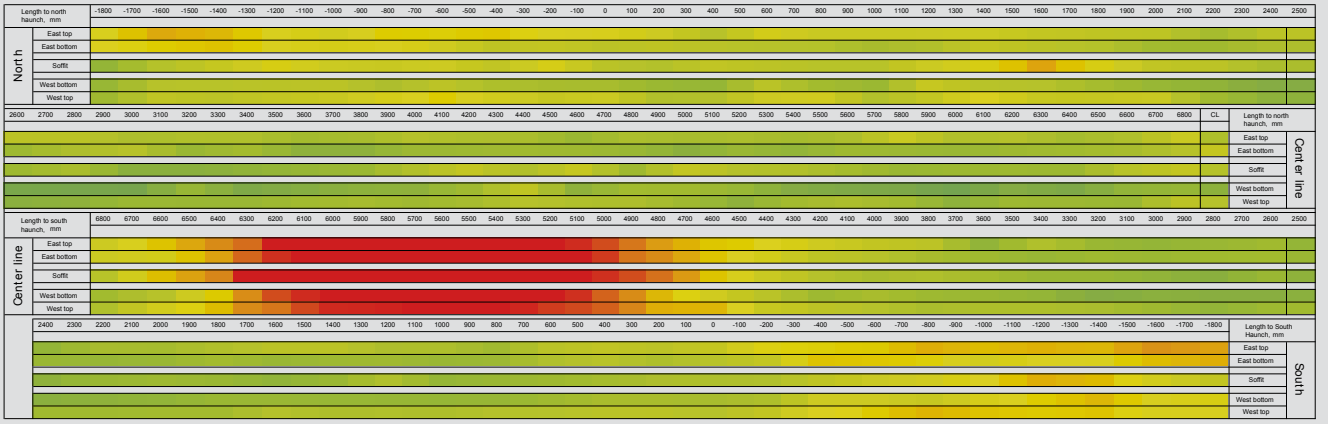

Figure 4. Electro-potential mapping results from beam 2C. Red regions indicate a high likelihood of corrosion. Note: 1 mm = 0.0394 in.

Concrete dust samples were collected for chloride content testing by drilling into the concrete and collecting drilling dust samples from measured depths. The acid-soluble chloride content of these samples was determined using dynamic end point potentiometric titration against 0.1 M silver nitrate solution. The analysis method was calibrated against results from a commercial laboratory complying with the method given in AS1012.20.3[13] Chloride content by mass of concrete was then plotted against depth to give the chloride profile, and the concentration at the depth of reinforcement was determined. As the chloride concentration at the depth of reinforcement increases, so does the probability that corrosion will initiate. For prediction purposes, a discrete threshold concentration is required as the point at which corrosion is deemed to initiate. This threshold value is disputed in the literature, and a range of values are suggested. ACI 222R[14] suggests values ranging from 0.026% to 0.06% by mass of concrete. Naito and Warncke suggested 0.032% in a 2008 report.[15] This study uses a threshold of 0.05%, which was suggested by The Concrete Society[16] and used by Bruce et al.[1] For beams that had not begun to corrode, the chloride profile and chosen chloride threshold were used to estimate the remaining time to initiation using a model based on Fick's Laws of Diffusion.[11]

More than 100 chloride profiles were collected and analyzed from Tiwai Point Bridge beams. The profiles were collected from beams removed from different areas of the bridge and from three to six locations on each beam so that critical areas of chloride buildup could be identified. These data are not presented here but will be used in a future study to assess the exposure conditions at the bridge site with an emphasis on identifying the effects of the different microclimates existing in different parts of the structure. Any observed trends will be used to predict critical locations on other structures so that bridge inspectors can more effectively target chloride analyses. It may also allow economies to be found in the design of new structures by optimizing durability design criteria throughout the structure.

Figure 5 gives an example of chloride ingress in the soffit of three beams. A considerable difference in chloride con-

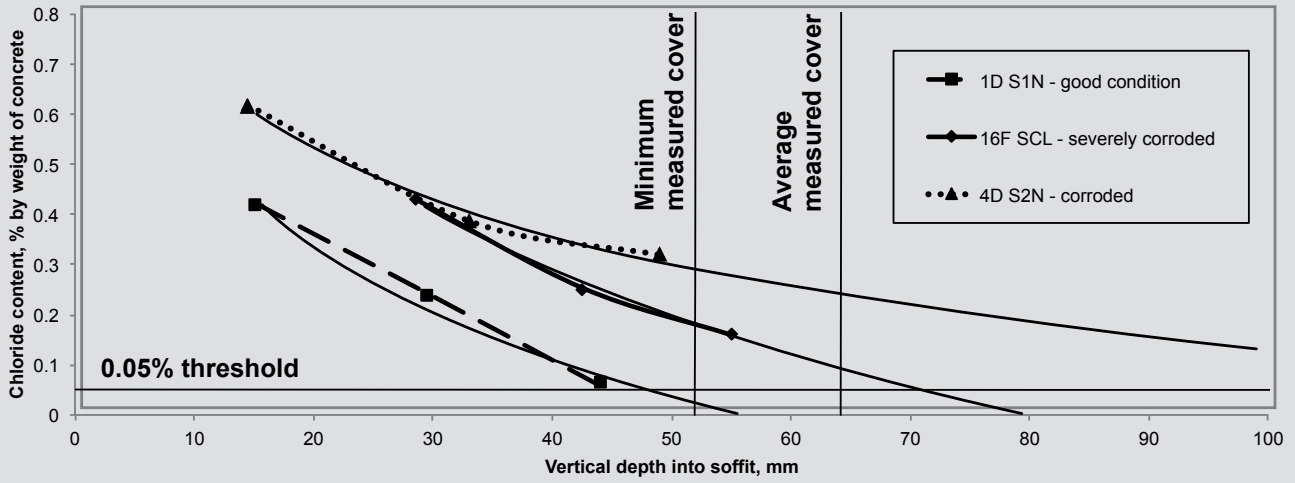

Figure 5. Preliminary chloride ingress results for three Tiwai Point Bridge beams of varying conditions. Note: 1 mm = 0.0394 in.

Broken-out strands with uniform corrosion

Individual wires with pitting damage

Figure 6. Examples of corroded pretensioned strands.

tent at the depth of reinforcement was observed between the beam in good condition and the two corroding beams. Chloride ingress testing is a useful tool for assessing the likelihood that corrosion of steel is occurring in a given beam and for estimating the time to initiation but is not useful for assessing the extent or location of corrosion in a beam that is known to be corroding. Full chloride ingress results are therefore excluded here because they do not aid in the assessment of residual strength of members.

Carbonation depth

Carbonation can contribute to reinforcement corrosion and occurs when airborne carbon dioxide penetrates the concrete and causes the pH to decrease to the level at which the alkalinity of the concrete no longer provides passivation for the reinforcing steel. Carbonation depth was measured by spraying a solution of phenolphthalein pH indicator onto a freshly cut concrete surface and measuring the depth of the color change.

Carbonation measurements were performed on 10 beams, and carbonation depths were found to be insignificant; the average carbonation depth was less than 5 mm (0.2 in.).

Concrete strength

Rebound hammer readings were taken on all beams to assess relative concrete strength. These readings were calibrated against a total of six cores taken from four different beams.

Typical average rebound hammer readings taken from the vertical face of the web were around 62. This is near to the upper limit for the device and converts to a compressive strength of greater than 58 MPa (8.4 ksi). Calibration of the rebound hammer values against measured compressive strength results from collected core samples is yet to be performed. However, the compressive strength of core samples was measured to be 66.5 MPa (9.64 ksi) in a 2004 inspection[17] and 69 MPa (10 ksi) and 56.7 MPa (8.22 ksi) on cores taken during destructive testing.

Condition assessment

Assessment of the condition of each beam requires an understanding of the process by which a single strand corrodes and the progression of the corrosion of strands within each beam. The beams with 12 pretensioned strands displayed a similar corrosion progression, which was different from that observed in beams with 10 pretensioned strands.

Corrosion of a single strand

There are a number of different mechanisms by which corrosion of a strand can occur.[1] These mechanisms are predominantly influenced by existing conditions in the surrounding concrete.

In the case of the Tiwai Point Bridge, corrosion was initiated by chloride ingress resulting from seawater being deposited on the surface of the concrete. Chloride-induced corrosion usually first initiates in a corner strand because they are exposed to chloride ingress from two sides. In sound concrete, corrosion of a strand will manifest either uniformly over the surface of the steel or as a concentrated pit. Both processes were observed on beams from the Tiwai Point Bridge (**Fig. 6**). As corrosion progresses, the expansion of the corrosion product eventually causes a longitudinal crack to form at the level of the corroding steel.[11] This crack causes a change in the surrounding concrete and thus in the corrosion process.

After longitudinal cracking of the concrete has occurred, seawater and oxygen are more readily available to the corroding steel and the process accelerates. The cracking usually causes debonding of the lower part of the strand because the concrete is less stiff in the direction of the soffit. This debonding forms a void below the strand where seawater collects (**Fig. 7**). The presence of seawater around the bottom of the strand causes the strand to corrode uniformly upward toward the top of the strand. This type of corrosion was widespread in cracked regions of the corroded test beams (right part of Fig. 7). Because each strand

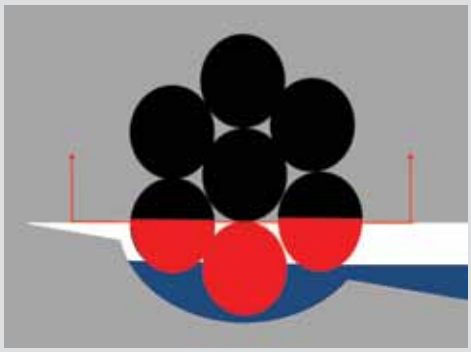

Corrosion progression of wires in a single strand

Corrosion-induced crack allowing water and air to bottom surface of corner strand

Evidence of upward strand corrosion

Figure 7. Upward pretensioned strand corrosion.

comprised six helical wires wrapped around a seventh straight central wire, all six of the helical wires rotate past the bottom of the strand in a length of less than 200 mm (7.87 in.). Combined with the compromised bond in corroded and cracked regions, it is not overly conservative to assume that 85% of the capacity of a strand is lost when corrosion has progressed one-third of the height of the strand, which correlates to a loss of approximately 30% of the strand's cross-sectional area. When corrosion has progressed to two-thirds of the height of the strand, 100% of the capacity is lost.

Because strands are made up of small wires, they corrode faster than conventional reinforcement bars. The corrosion is accelerated for three main reasons:

- The voids between the wires allow moisture and chlorides to build up and propagate easily.
- Corrosion attacks the available steel surface, and strands have a high specific surface.
- The high stress in the steel may increase the rate of corrosion compared with conventional reinforcing.

The combination of processes described in this section results in the load-carrying ability of a strand being rapidly reduced to effectively zero once a crack reaches it sand debonding occurs. For this reason, any strand that is determined to be intersected by a longitudinal crack should be assumed to be ineffective and should be neglected in the calculation of residual strength of the beam. This approach is only slightly conservative and is more accurate than estimating the percentage of cross section lost and assuming that the remaining cross section is effective.

Progression of corrosion in a beam

As corrosion in the corner strand progresses from the situation shown in Fig. 7 (bottom left), the crack widens and propagates farther horizontally across the beam soffit. In the beams with 12 pretensioned strands, 4 strands were present in the bottom layer. In these beams the crack intersected the adjacent strand in the bottom layer where the debonding and upward corrosion process began again. Because both sides of each beam's web are subjected to similar exposure environments and concrete conditions, many of the beams had this process occurring concurrently on both sides of the web. This process repeats until the crack reaches the entire width of the web and the soffit concrete is completely delaminated. **Figure 8** shows this sequence diagrammatically, and **Fig. 9** gives an example of a beam after the delaminated soffit had fallen away during the destructive test, with evidence of strand corrosion visible on the spalled concrete section.

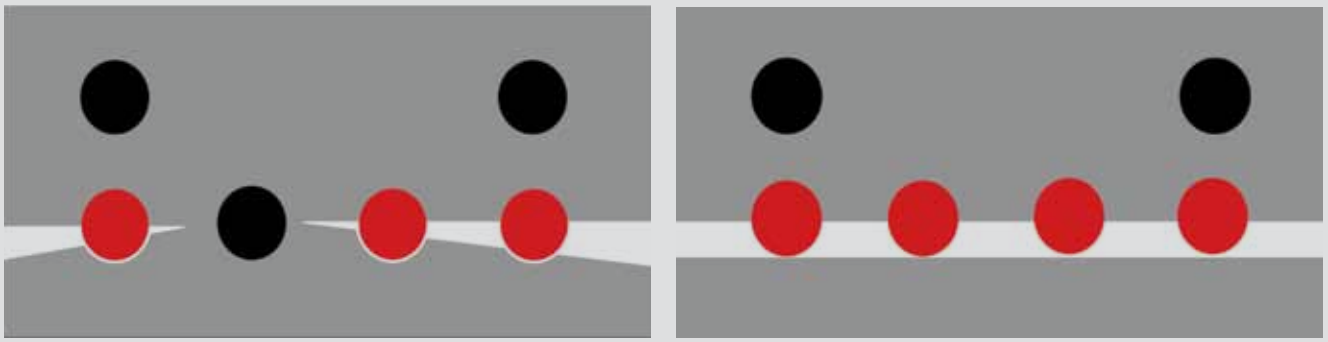

Figure 8. Progression of cracking and delamination due to corrosion of pretensioned strands in a beam.

In the beams with 10 pretensioned strands there were only two strands on the edges of the bottom layer, so the crack did not intersect another strand but instead propagated downward to the soffit and caused the corner concrete to spall. This exposed the corroding strand to the atmosphere, allowing chloride ingress to occur on the freshly exposed concrete surface and reducing the time to initiation for the next strand.

Condition assessment methodology

The proposed methodology for assessing the condition of the corroded beams is based on assessing which stage of the cracking and debonding progression a given beam has reached. As explained in the previous sections, once a crack has intersected a strand it is assumed that the strand has lost its load-carrying ability at the affected section.

Figure 9. Evidence of soffit delamination during a destructive test.

The presence of a longitudinal crack on one side of a web implies that at least the nearest strand is corroding and has been intersected by the crack. The width of the crack and the EPM results taken from areas surrounding the crack can indicate the severity of the corrosion and thus can be used to assess the likelihood that the crack has propagated and intersected the second and third strands.

By the time the crack has propagated to intersect the fourth strand, only a small amount of sound concrete remains, so it is likely that delamination of the soffit would have occurred due to tensile forces caused by opening of the crack. For this reason, if a longitudinal crack is only visible on one side of the web it is fair to assume that at least one strand on the opposite side is intact.

The presence of longitudinal cracks on both sides of the web at a given section implies that at least the shallowest strand on both outside edges is corroding and at worst that the soffit has delaminated, exposing the entire layer of strands. The soffit should be checked for delamination by sounding with a hammer. If delamination has occurred, all four strands are intersected by the crack and should be neglected in the calculation of residual strength. If delamination has not occurred, it is likely that at least one of the two central strands is not corroding, so one strand can be assumed to be effective. However, it is expected that a beam in this condition will quickly deteriorate to full delamination.

Residual strength assessment

Background

There exists a knowledge gap surrounding the assessment of the strength of concrete beams that have experienced pretensioned reinforcement corrosion. One factor contributing to this gap was a shortage of destructive test data from corroded pretensioned concrete bridge beams. A lack of data makes accurate assessment of the residual strength of beams difficult and often leads to bridges being replaced rather than rehabilitated. The strength assessment of corroded pretensioned beams is more complicated than for conventionally reinforced concrete beams because corrosion can cause relaxation of the steel and also compromises the integrity of the bond between the steel and concrete. Both of these effects reduce the amount of prestress that is transferred to the concrete and thereby weaken the structure considerably.

The bond between the steel and concrete is a difficult parameter to measure accurately even on a strand-by-strand basis, let alone for an entire beam or bridge. The difficulty of accurate assessment of bond characteristics makes assessment of the residual strength of a corroded pretensioned beam difficult and makes strengthening operations to restore lost prestressing force dangerous due to the risk of overstressing the concrete member.

Objectives and outcomes

The major objective of the residual strength assessment was to provide a correlation between nondestructive assessment methods and the measured strength of corroded pretensioned concrete bridge beams. This correlation was achieved by generating a large number of data points that relate the findings of a variety of nondestructive bridge assessment techniques to the measured flexural performance of full-scale decommissioned concrete bridge beams.

The secondary objective was to generate information for a direct comparison tool that will be used by bridge consultants in the assessment of beams that have experienced pretensioned reinforcement corrosion. The information to be included in the tool is summarized here.

Scope

The assessment consisted of destructive and nondestructive testing of 19 beams that had experienced different degrees of corrosion to the pretensioned strand. Beams were selected for testing based on their prestressing design, location on the bridge, and degree of corrosion as assessed visually.

Results

Nondestructive testing results are summarized, along with data observed after breaking out concrete following destructive testing. Results of EPM provide a good correlation with corrosion damage and failure location, though in most cases the corrosion damage and failure location were also identified by visual inspection. No strand corrosion was detected with EPM in areas that had not experienced cracking, which is consistent with the behavior of the beams during destructive testing; no strand breakages were detected outside of areas that had been identified as corroded using nondestructive means.

Comparison of the crack patterns present on each beam with the number of corroded strands identified after breakout correlates well with the condition assessment methodology described in the previous section. All of the beams with cracking visible on both sides of the web had corrosion damage to either three or four of the strands in the bottom layer, while those beams with cracking on only one side (or on both sides but not at the same section) had damage to between one and three strands.

Destructive testing

Destructive testing was performed on beams with three of the four prestressing arrangements as described in the design and construction section, and the results from each of the groups were analyzed independently. Selection of beams for each group was performed by grading based on the amount of longitudinal cracking evident on the sides

Table 2. Summary of destructive tests

Description of beam type	Good condition	Corroded pretensioning	Total tests
12 pretensioned strands without expansion joint	2	4	6
12 pretensioned strands with expansion joint	2	3	5
10 pretensioned strands without expansion joint	2	1	3
No expansion joint and cut pretensioned strand	1	0	1
Expansion joint and cut pretensioned strand	1	0	1
10 pretensioned strands and cut posttensioned tendon	1	0	1
Data requires further postprocessing	1	1	2

of the web. The condition of each test beam was confirmed after testing by breaking out areas of concrete to expose reinforcement. **Table 2** summarizes the 19 tests.

Test setup

The beams were tested in a simply supported state using a four-point loading system. Due to the remote location of the bridge, the large size of the test specimens, and the extensive testing regime, the cost to transport and test the beams at a laboratory was prohibitive. The testing was therefore performed on-site using a purpose-built self-reacting load frame constructed from four of the decommissioned bridge beams, a steel yoke, and tension ties. The rig was designed to cause flexural failure in the specimens and to approximate an axle loading condition. **Figure 10** shows the test setup.

The destructive testing phase commenced after the nondestructive testing phase and was concurrent with deconstruction of the second half of the bridge. As the deconstruction of the bridge continued, the final test beams were selected and the remaining nondestructive tests performed on those beams.

Load was applied to the asphalt surfacing on the test beams through two 100 mm wide (4 in.) line loads oriented across the width of the flange. The line loads were located 1.5 m (4.9 ft) either side of midspan and were applied through a simply supported spreader beam by a single 1000 kN (225 kip) hydraulic ram at midspan. Load was measured using a load cell on the ram, and deflections were measured relative to the ground below each of the line loads. Deflection of the end supports was also measured relative to the ground, and the beam deflections were adjusted to account for this support deflection. Load readings did not take into account the self-weight of the beams.

Acoustic emissions monitoring equipment was used to detect damage during the destructive testing. The acous-

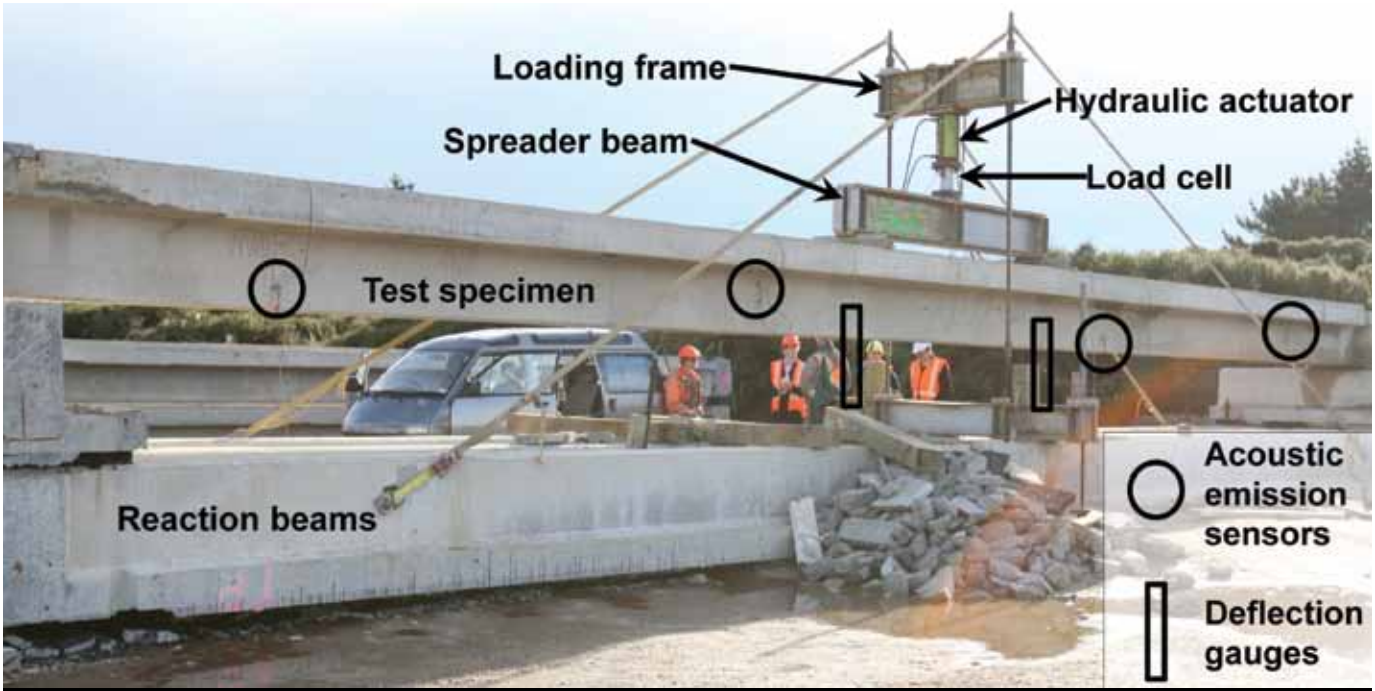

Figure 10. Self-reacting loading frame and instrumentation for destructive testing.

Figure 11. Test rig and deflected good-condition beam.

tic emissions system was deployed to identify and locate prestressing strand breakage during the destructive tests so that these data could be compared with corrosion sites identified by nondestructive testing. The acoustic emissions data were time stamped and recorded concurrently with load and deflection data. Failure of reinforcement, both stressed and nonstressed, was only detected in strands that experienced severe corrosion. Failed strands were located exclusively in the bottom or second layer of pretensioned reinforcement, with the majority in the bottom layer. Failed strands were only detected in areas that exhibited external evidence of corrosion.

Test rig construction

The tests were performed in a number of stages scheduled to fit into the deconstruction program. The first stage involved the construction of the components required for the destructive loading frame. This process involved the manufacture of four heavy steel beams, which, along with several high tensile rods, formed the central part of the frame. Four of the bridge beams were prepared to form the longitudinal reaction beams and end supports. The three bridge beams selected to be used as reaction beams were rolled upside down and positioned, with care taken to ensure that they were supported near midspan to maintain a similar gravity load profile and counteract the prestress moment. The fourth beam was cut into sections and positioned across the ends of the reaction beams to form the supports. The lower part of the central tower was then assembled, the end support beam sections were located and fixed, and the first test unit was positioned on the rig. The spreader beam was placed on top of the test unit. The top part of the tower and actuator was assembled on the ground and then lifted onto the test rig and attached using couplers on the vertical high tensile rods and ratchet strops for stability. **Figure 11** shows the completed test rig.

Loading procedure

The loading procedure for the beams was complicated by the limited stroke of the hydraulic ram. The stroke capacity of the jack was approximately 250 mm (10 in.), and the beams failed at deflections of approximately 400 mm (16 in.). For this reason the beams were loaded to full stroke and then propped using timber struts (Fig. 11). The hydraulic ram was then retracted and a packer inserted, allowing the load to be reapplied through the packer once the timber struts were removed. This process was repeated until sufficient deflection capacity was made available. This loading procedure resulted in the load cell reading's dropping to zero as the load was transferred to the timber struts while the beam remained deflected. This portion of the data has been removed from the load-deflection graphs to reduce clutter but is evident from the two small drops in load at approximately 225 mm (9 in.) and 250 mm (10 in.) deflection.

Failure modes

The load-deflection response of all three beam types was similar. Good-condition beams deflected evenly and displayed regularly spaced vertical flexural cracks located over the middle third of the span. Some beams in good condition also displayed a pure web shear crack approximately 2 m (6.6 ft) from the support point, just outside the haunch of the beam. The shear cracks coincided with the end of the debonding of the bottom four to six pretensioned strands. In all but two cases the beams that were in good condition failed at one of the loading points with a flexural shear crack extending from outside the loading point and penetrating

Figure 12. Typical good-condition failure crack.

into the flange, followed by crushing of the concrete in the compression zone. In the two exceptional cases, the beam displayed a shear failure beginning 2 m (6.6 ft) from the end of the beam and spreading to the nearest load point. **Figure 12** gives an example of the typical failure mode for the good condition beams. Concrete crushing was evident under the loading point, and the longitudinal reinforcement is intact and visible where the cracked concrete in the tension zone fell away during failure of the beam. The acoustic emissions system detected no strand breakage during the good condition tests, and this result was confirmed by post-test breakout and inspection around the failure plane.

The curvature of deflected beams with corrosion damage was typically concentrated around the damaged area. Flexural cracking would extend up and outward from the original corrosion crack, and the soffit would spall off at a small deflection. The acoustic emission system did not detect any strand failures outside of the corroded area that ultimately failed. **Figure 13** shows a typical cracking pattern for a corroded beam (top left and top right). Usually failure would occur at a loading point, with the failure crack extending from the corroded area to meet the loading point (Fig. 13 bottom left and bottom right). If the corroded area was too far away from the loading point, the strands would fail at the corroded section and then pull through to a separate failure crack closer to the loading point (Fig. 13 bottom right).

Control tests and comparison of prestressing arrangements

Destructive testing was performed on three of the four different prestressing arrangements on the bridge. **Figure 14** compares beams in good condition containing each of the three different prestressing arrangements that were subjected to testing. These beams displayed similar ductility characteristics and a 12% difference in ultimate load between the strongest and weakest of those tested, with the fourth prestressing type expected to be the weakest.

Three control tests were also conducted to isolate the two differing posttensioned tendon drapes and the pretensioned reinforcement. The control tests were performed by cutting all of either the pretensioned or the posttensioned reinforcement to isolate the other. The reinforcement was cut as close as possible to the failure locations displayed by full-strength beams. Figure 14 gives load-deflection plots from the control tests, showing that the strength contribution from the pretensioned strand is considerably greater than that from the posttensioned tendon and that the two different drapes resulted in a small difference in strength.

12 pretensioned strands without expansion joint

Six tests were performed on beams with 12 pretensioned strands and no expansion joint, with two tests on good-condition beams and four tests on beams displaying corrosion damage to the pretensioned reinforcement. **Figure 15** displays the six load-deflection plots. The average ultimate strength of the beams in good condition was 342.5 kN (77.00 kip), whereas the weakest of the corroded beams supported only 68% of this load. Posttest inspection revealed that the weakest beam (2C) had corrosion damage to all four strands in the bottom layer of pretensioned reinforcement, evidenced by a 1200 mm (47 in.) crack 1.5 m (4.9 ft) from midspan that was visible on both sides of the web. As stated in Table 1, beams 18E and 3D also had corrosion damage to all four bottom strands, while 21F had corrosion damage to three.

Delamination of soffit in corroded region

Typical cracking pattern emanating from corroded area

Failure crack location emanating from corroded area to loading point

Corroded strands failed and pulled through to separate failure crack at loading point

Figure 13. Typical corroded beam cracking and failure.

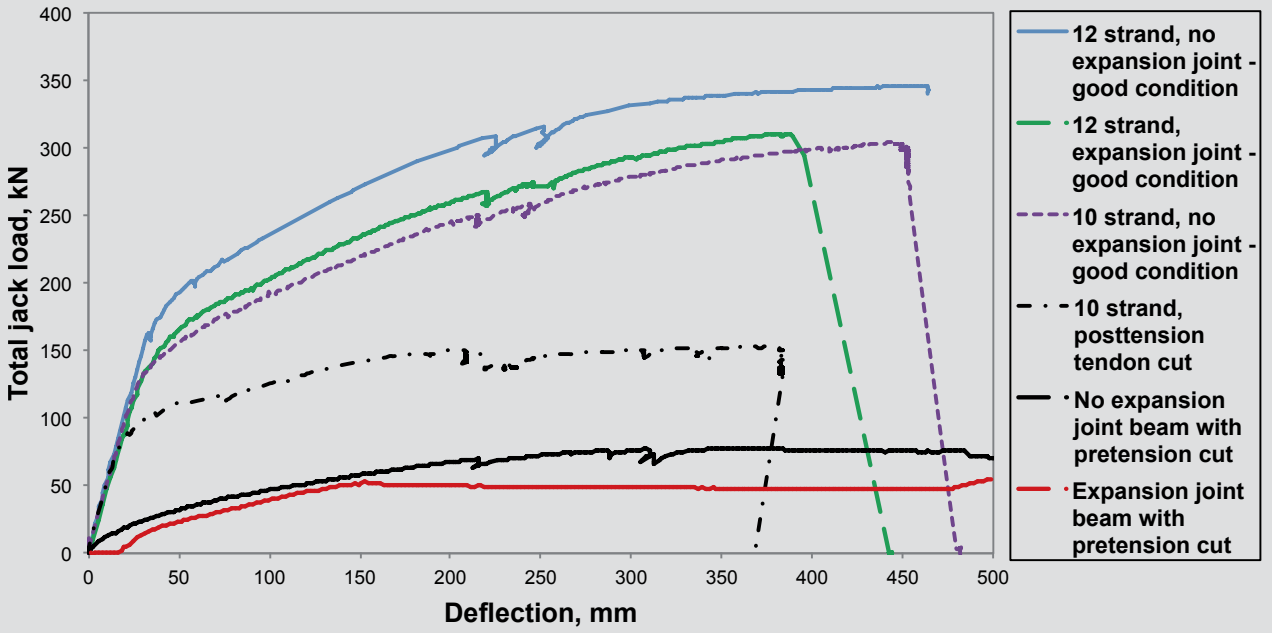

Figure 14. Control test results and prestressing arrangement comparison. Note: 1 mm = 0.0394 in.; 1 kN = 0.225 kip.

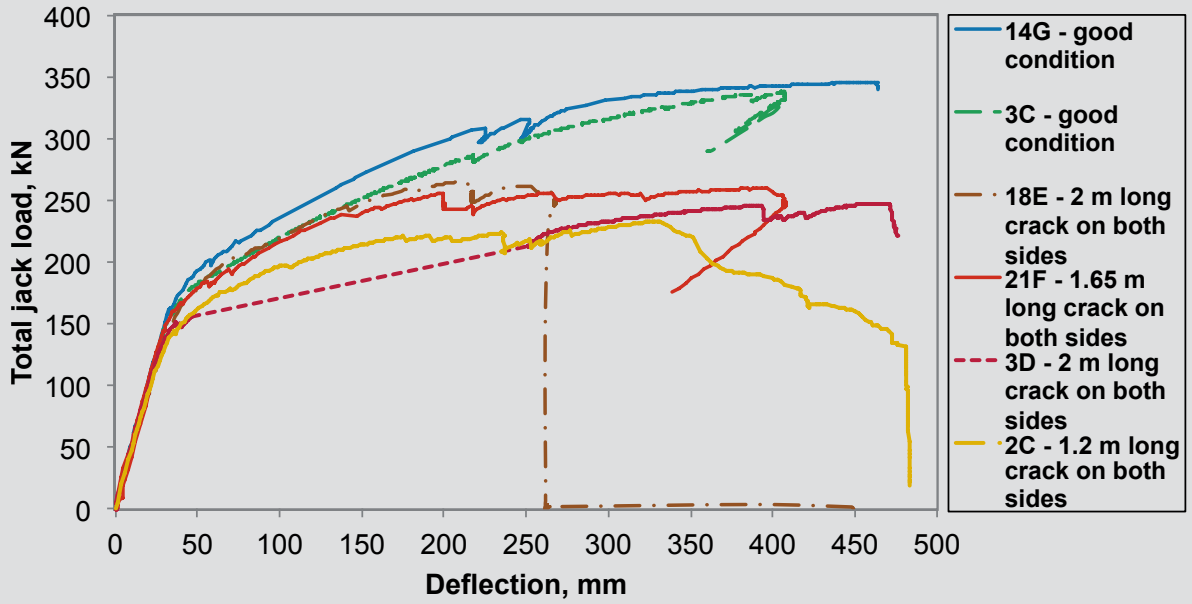

Figure 15. Load versus deflection for 12 pretensioned strands with no expansion joint. Note: 1 mm = 0.0394 in.; 1 m = 3.28 ft; 1 kN = 0.225 kip.

12 pretensioned strands with expansion joint

Five tests were performed on beams with 12 pretensioned strands and an expansion joint. Two tests were on beams in good condition and three tests were on beams displaying corrosion damage to the pretensioned reinforcement. **Figure 16** displays load-deflection plots from these five. The average ultimate strength of the beams in good condition was 313.5 kN (70.48 kip), whereas the weakest of the corroded beams supported only 69% of its good condition counterpart. Posttest inspection revealed that the weakest beam (16F) had corrosion damage to all four strands in the bottom layer of pretensioned reinforcement, which was evidenced by cracking and spalling of the lower part of the web and soffit over a length of 2.2 m (7.3 ft) extending outward from near to midspan. The other corroded beams (4D and 16G) had corrosion damage to three of the four strands in the bottom layer.

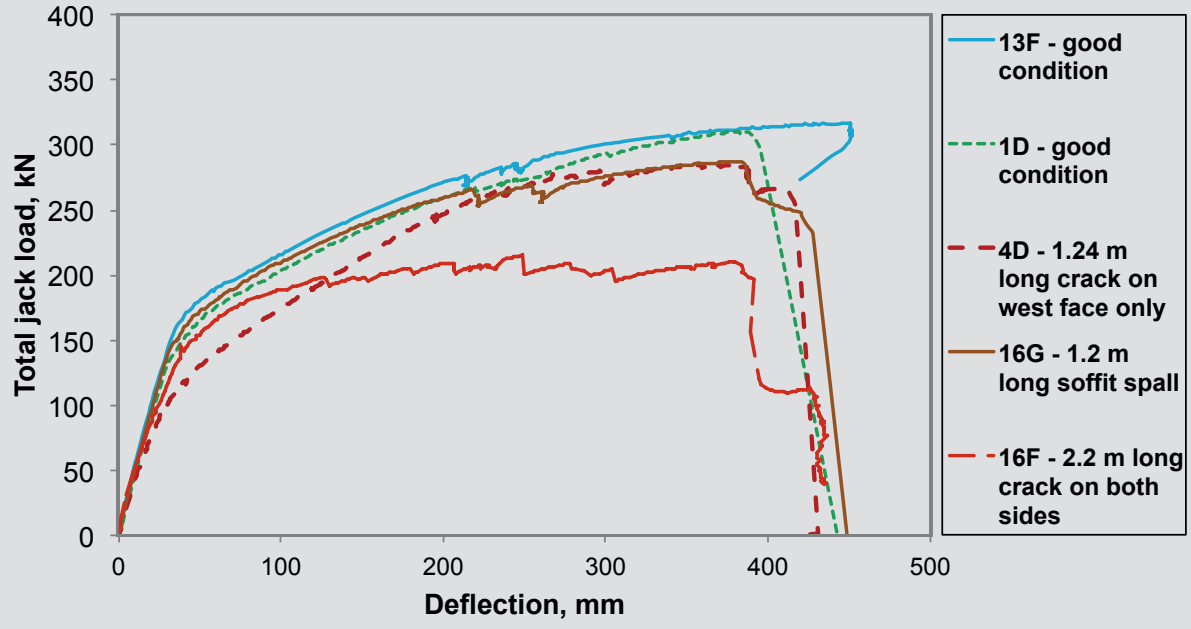

Figure 16. Load versus deflection for 12 pretensioned strands with expansion joint. Note: 1 mm = 0.0394 in.; 1 m = 3.28 ft; 1 kN = 0.225 kip.

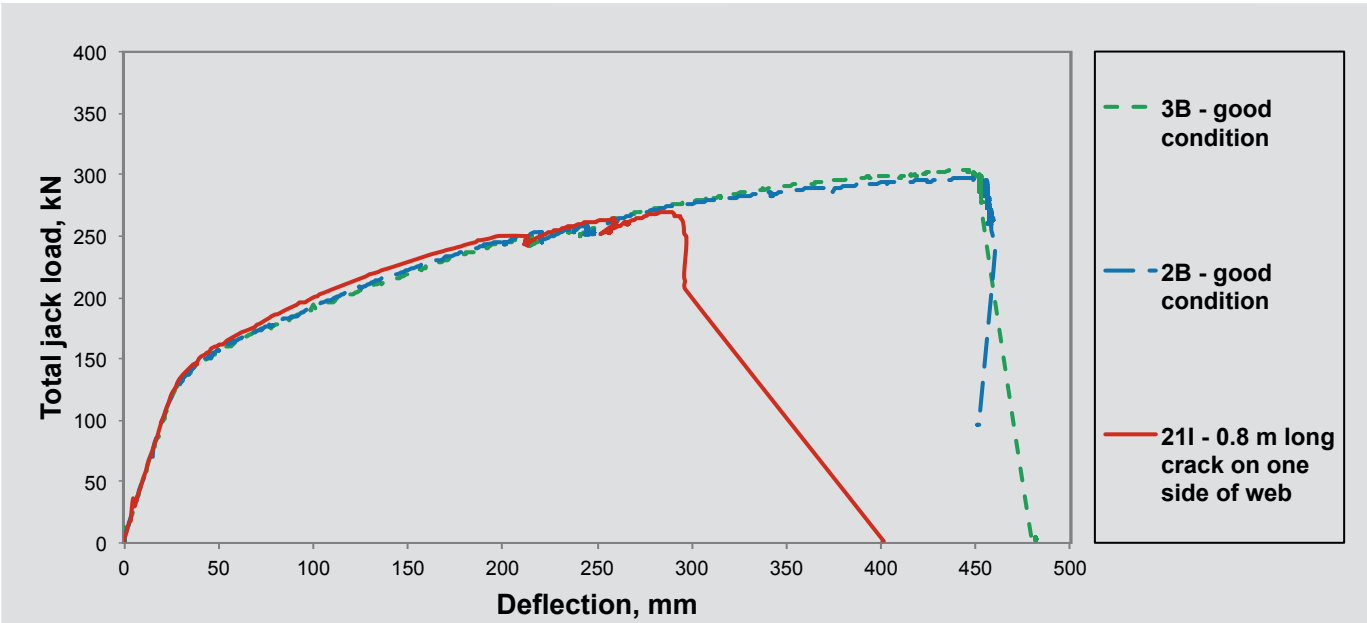

Figure 17. Load versus deflection for 10 pretensioned strands with no expansion joint. Note: 1 mm = 0.0394 in.; 1 m = 3.28 ft; 1 kN = 0.225 kip.

10 pretensioned strands without expansion joint

Three tests were performed on beams with 10 pretensioned strands and no expansion joint. Two tests were on beams in good condition and one test was on a beam displaying corrosion damage to the pretensioned reinforcement.

Figure 17 displays load-deflection plots of these three tests. The average ultimate strength of the beams in good condition was 301 kN (67.7 kip), whereas the corroded beam sustained 90% of its good-condition counterpart. This weaker beam (21I) had corrosion damage to one of the two pretensioned strands in the bottom layer of reinforcement, which was evidenced by an 800 mm long (31.5 in.) crack visible on only one side of the web.

Conclusion

Accurate assessment of the residual strength of concrete bridge beams with corroding pretensioned reinforcement is a complex problem, and few data points from full-scale destructive tests exist in the literature. This project provides a comparatively large number of data points relating destructive and nondestructive condition assessments to measured flexural strength for beams of similar design with varying degrees of corrosion damage. These data points will be used in a later study for the development and assessment of general methods for evaluation of the residual strength of in-service structures with corroding pretensioned reinforcement.

Destructive tests were conducted on 19 beams with three different designs from the Tiwai Point Bridge. Good-condition beams of the same design displayed similar load-deflection behavior. All beams that displayed corrosion of the pretensioned reinforcement had reduced capacity, with strength loss being approximately proportional to the number of strands affected by corrosion. The worst-condition beams had damage to all four strands in the bottom layer and achieved strengths of 68% and 69% of their good-condition counterparts.

The actual damage to the reinforcement assessed by breakouts after destructive testing was compared with the condition assessment methodology that was developed for the assessment of the beams using nondestructive testing methods.

Using only the data from the nondestructive tests, the methodology was shown to provide an effective means of estimating the number of corroded strands that should be disregarded in calculation of the residual strength of a damaged beam. All of the beams with cracking visible on both sides of the web had corrosion damage to either three or four of the strands in the bottom layer, while those beams with cracking on only one side (or on both sides but not at the same section) had damage to between one and three strands.

Acknowledgments

The authors are grateful for the guidance and expertise provided by Sheldon Bruce of Opus International Consultants Ltd. and Michael Lawson of Construction Techniques Ltd. The experiments described in this paper were conducted with the permission of the Invercargill City Council on a Fulton Hogan Ltd. site and with the assistance of Fulton Hogan staff and equipment. Financial support was provided by the New Zealand Transport Agency.

References

1. Bruce, S. M., P. S. McCarten, S. A. Freitag, and L. M. Hasson. 2008. *Deterioration of Prestressed Concrete Bridge Beams*. Land Transport New Zealand research report 337. Wellington, New Zealand: Land Transport New Zealand.

2. Pape, T. 2008. "Investigating the Correlation between Pre- and Post-demolition Assessments for Precast, Post-tensioned Beams in Service for 45 Years." PhD thesis, University of Newcastle Australia.

3. Harries, K.A. 2009. "Structural Testing of Prestressed Concrete Girders from the Lake View Drive Bridge." *Journal of Bridge Engineering* 14 (2): 7892. http://ascelibrary.org/beo/resource/1/jbenf2/v14/i2/p78_s1?view=fulltext.

4. Thomas, C., and G. Coles. 2006. *Tiwai Bridge Options Study.* Report number C/5/392. Invercargill, New Zealand: MWH New Zealand Ltd.

5. Opus International Consultants Ltd. 2007. *Invercargill City Council Tiwai Bridge Superstructure Replacement.* Design drawing number 6/584/22-3604 Sheet 1 held at Invercargill City Council. Christchurch, New Zealand: Opus International Consultants Ltd.

6. Inglis, G., N. Gust, I. Fitridge, O. Floerl, C. Woods, B. Hayden, and G. Fenwick. 2005. *Port of Bluff: Baseline Survey for Non-indigenous Marine Species.* Wellington, NZ: New Zealand Ministry of Agriculture and Forestry. http://www.biosecurity.govt.nz/files/pests/salt-freshwater/2005-07-port-of-bluff.pdf.

7. U.K. National Meteorological Library and Archive. 2010. *Fact Sheet 6 — The Beaufort Scale.* Devon, U.K.: Met Office. http://www.metoffice.gov.uk/media/pdf/4/4/Fact_Sheet_No._6_-_Beaufort_Scale.pdf.

8. Thomas, C., and G. Coles. 2006. *Tiwai Bridge Posting Review.* Report Z1243301. Invercargill, New Zealand: MWH New Zealand Ltd. for the Invercargill City Council.

9. Consulting Engineers: Powell Fenwick & Partners. 1968. Design drawing number ICC 5946/2B. In *Tiwai Bridge Alternative.* Wellington, New Zealand: Wilkins & Davies Construction Co. Ltd.

10. Thomas, C., and G. Coles. 2008. *Tiwai Bridge Visual Inspection*. Report 801/009194 Invercargill, New Zealand: MWH New Zealand Ltd. for the Invercargill City Council.

11. Broomfield, J. P. 1997. *Corrosion of Steel in Concrete: Understanding, Investigation and Repair.* London, UK: E & FN Spon.

12. Naito, C., L. Jones, and I. Hodgeson. 2010. *Inspection Methods and Techniques to Determine Non Visible Corrosion of Prestressing Strands in Concrete Bridge Components: Task 3 — Forensic Evaluation and Rating Methodology.* Bethlehem, PA: ATLSS. http://www.trb.org/Main/Blurbs/163798.aspx.

13. AS 1012.20. 1992. *Methods of Testing Concrete: Method 20: Determination of Chloride and Sulfate in Hardened Concrete and Concrete Aggregates*. Sydney, Australia: Standards Australia.

14. ACI (American Concrete Institute) 222R. 2001. *Protection of Metals in Concrete against Corrosion.* Farmington Hills, MI: ACI.

15. Naito, C., and J. Warncke. 2008. *Inspection Methods and Techniques to Determine Non Visible Corrosion of Prestressing Strands in Concrete Bridge Components: Task 1 — Literature Review.* Bethlehem, PA: ATLSS. http://trid.trb.org/view.aspx?id=924782

16. Concrete Society. 1984. *Repair of Concrete Damaged by Reinforced Corrosion.* Concrete Society technical report 26. Blackwater, UK: Concrete Society.

17. Thomas, C., and D. Kensington. 2004. *Tiwai Bridge Evaluation and Repair Design*. Report RICC01. Invercargill, New Zealand: MWH New Zealand Ltd. for the Invercargill City Council.

About the authors

Rhys Rogers graduated from the University of Auckland with a BE in civil engineering in 2008 and is soon to complete a PhD at the same institution. His doctoral research focuses on the durability of pretensioned, precast concrete bridges in New Zealand, with particular attention paid to corrosion of pretensioned reinforcement due to chloride ingress. Rhys's research interests include both structural and durability engineering, and he has been involved in a number of research projects in these fields in addition to his doctoral research.

Liam Wotherspoon is the EQC Research Fellow in the Department of Civil and Environmental Engineering at the University of Auckland in New Zealand. He received his BE and PhD in civil engineering from the University of Auckland in 2003 and 2009, respectively. His research interests include the seismic performance of bridges and ports and integrated modeling of structures and foundations.

Allan Scott, PhD, PEng, is a senior lecturer in the Department of Civil and Natural Resources Engineering at the University of Canterbury in Christchurch, New Zealand.

Jason M. Ingham, PhD, MBA, is an associate professor and deputy head of department (research) at the University of Auckland, New Zealand, and is currently president of the New Zealand Concrete Society and *fib* (International Federation for Structural Concrete) head of Delegation for New Zealand.

Abstract

Destructive tests were performed on 19 decommissioned pretensioned concrete bridge beams that had corroded pretensioned reinforcement. The beams were obtained from the 1969 Tiwai Point Bridge in Southland, New Zealand, which experienced chloride-induced corrosion caused by sea spray that resulted in the superstructure's being decommissioned and removed in 2009. Destructive flexural testing results were compared with thorough nondestructive condition assessments and with post-test breakouts of reinforcement. The beams tested ranged from good-condition beams to those with severe corrosion in 4 of the 21 prestressed strands. The most severely corroded beam sustained 69% of the load of an equivalent good-condition beam. A proposed methodology for the assessment of the residual strength of beams with corroded pretensioned reinforcement was shown to provide an effective means of estimating the number of corroded strands that should be disregarded in the calculation of the residual strength.

Keywords

Chloride, corrosion, girder, pretension, testing.

Review policy

This paper was reviewed in accordance with the Precast/Prestressed Concrete Institute's peer-review process.

Reader comments

Please address any reader comments to journal@pci.org or Precast/Prestressed Concrete Institute, c/o *PCI Journal*, 200 W. Adams St., Suite 2100, Chicago, IL 60606.